Acta Crystallographica Section D
Biological Crystallography
ISSN 1399-0047

Molecular mechanism for self-protection against the type VI secretion system in *Vibrio cholerae*

Xuan Yang,[a]‡ Min Xu,[b]‡ Yanying Wang,[a] Pengyan Xia,[a] Shuo Wang,[a] Buqing Ye,[a] Liang Tong,[c]* Tao Jiang[b]* and Zusen Fan[a]*

[a]Chinese Academy of Sciences Key Laboratory of Infection and Immunity, Institute of Biophysics, Chinese Academy of Sciences, Beijing 100101, People's Republic of China, [b]National Laboratory of Biomacromolecules, Institute of Biophysics, Chinese Academy of Sciences, Beijing 100101, People's Republic of China, and [c]Department of Biological Sciences, Columbia University, New York, NY 10027, USA

‡ XY and MX contributed equally to this work.

Correspondence e-mail: ltong@columbia.edu, tjiang@ibp.ac.cn, fanz@moon.ibp.ac.cn

Received 22 November 2013
Accepted 17 January 2014

PDB reference: VgrG3C^{CD}–TsiV3 complex, 4noo

VgrG proteins form the spike of the type VI secretion system (T6SS) syringe-like complex. VgrG3 of *Vibrio cholerae* degrades the peptidoglycan cell wall of rival bacteria *via* its C-terminal region (VgrG3C) through its muramidase activity. VgrG3C consists of a peptidoglycan-binding domain (VgrG3C^{PGB}) and a putative catalytic domain (VgrG3C^{CD}), and its activity can be inhibited by its immunity protein partner TsiV3. Here, the crystal structure of *V. cholerae* VgrG3C^{CD} in complex with TsiV3 is presented at 2.3 Å resolution. VgrG3C^{CD} adopts a chitosanase fold. A dimer of TsiV3 is bound in the deep active-site groove of VgrG3C^{CD}, occluding substrate binding and distorting the conformation of the catalytic dyad. Gln91 and Arg92 of TsiV3 are located in the centre of the interface and are important for recognition of VgrG3C. Mutation of these residues destabilized the complex and abolished the inhibitory activity of TsiV3 against VgrG3C toxicity in cells. Disruption of TsiV3 dimerization also weakened the complex and impaired the inhibitory activity. These structural, biochemical and functional data define the molecular mechanism underlying the self-protection of *V. cholerae* and expand the understanding of the role of T6SS in bacterial competition.

1. Introdoction

Microbes have evolved a spectacular range of measures to compete for niches, to gain fitness and to pass on their genes (Hibbing *et al.*, 2010). Among the most sophisticated strategies are protein-secretion systems. The type VI secretion system (T6SS) has recently been shown to be a delicate system involved in bacterial competition (Hood *et al.*, 2010), injecting toxins into eukaryotic or prokaryotic recipient cells through a contact-dependent killing mechanism (Silverman *et al.*, 2012). Although T6SS is found in more than a quarter of Gram-negative bacteria with sequenced genomes (Bingle *et al.*, 2008), the effectors involved have been studied in only a small subset of T6SSs (Silverman *et al.*, 2012) and the cognate immunity proteins that neutralize the effectors have only been experimentally characterized in a few pathogenic bacteria, including *Pseudomonas aeruginosa* (Hood *et al.*, 2010), *Burkholderia thailandensis* (Russell *et al.*, 2012), *Serratia marcescens* (English *et al.*, 2012) and *Vibrio cholerae* (Pukatzki *et al.*, 2006).

V. cholerae has claimed millions of lives in the past century and is still pandemic in many parts of the world (Patrick, 2013; Vezzulli *et al.*, 2008). Efficient killing of a representative group of Gram-negative bacteria including *Escherichia coli* by *V. cholerae* depends on the T6SS (MacIntyre *et al.*, 2010). T6SS-positive (T6SS^{+}) *V. cholerae* sister cells are found in frequent conflict with each other, described as 'T6SS duelling'

behaviour (Basler & Mekalanos, 2012), and immunity proteins are required for the survival of T6SS$^+$ *V. cholerae*.

Valine glycine-repeat protein G (VgrG) is a hallmark of T6SS, structurally resembling the bacteriophage T4 gp5–gp27 complex (Supplementary Fig. S1;[1] Leiman *et al.*, 2009). VgrG trimerizes and forms the spike of the syringe-like structure and is required for the assembly and function of all known T6SSs (Shneider *et al.*, 2013). *V. cholerae* encodes three VgrG proteins, VgrG1, VgrG2 and VgrG3 (Supplementary Fig. S1), amongst which VgrG2 is the shortest and represents the 'core' VgrG composed of the gp27-like and gp5-like domains, while VgrG1 employs its accessory actin cross-linking domain (ACD) to resist engulfment by eukaryotic predators (Pukatzki *et al.*, 2007; Ma *et al.*, 2009; Durand *et al.*, 2012). VgrG3 contains a putative peptidoglycan-binding (PGB) domain in the C-terminal region, providing the first clue that the VgrG3-containing T6SS might target prokaryotes (Pukatzki *et al.*, 2007), which is a prerequisite for bacterial competition.

A systematic mutagenesis study of T6SS genes in *V. cholerae* identified three immunity proteins (TsiV1, TsiV2 and TsiV3; Dong *et al.*, 2013), whose corresponding effector proteins are TseL, VasX and VgrG3. The effector of VgrG3 is a lysozyme-like domain located in its C-terminal extension (VgrG3C), consisting of a peptidoglycan-binding domain (VgrG3C^{PGB}) and a putative catalytic domain (VgrG3C^{CD}) (Supplementary Fig. S1). VgrG3C targets the cell wall of bacterial prey for enzymatic digestion (Dong *et al.*, 2013, Brooks *et al.*, 2013). However, the molecular mechanisms of how TsiV3 inhibits the activity of VgrG3 and functions as an immunity protein remain elusive. Here, we present the first crystal structure of the VgrG3C^{CD}–TsiV3 complex at 2.3 Å resolution, as well as detailed biochemical, biophysical and functional studies to delineate the structural basis for self-protection in *V. cholerae*.

2. Methods

2.1. Protein expression and purification

The gene fragment encoding TsiV3 (VCA0124; residues 25–122) without the predicted 24-amino-acid N-terminal periplasm localization signal was cloned into pRSFduet vector ORF2 between *Nde*I and *Xho*I sites, with a redundant Met at the N-terminus. The gene sequence of VgrG3C (VCA0123; residues 728–1017) was then cloned into ORF1 of the pRSFduet vector with TsiV3 in ORF2 *via* *Bam*HI and *Sal*I sites, along with an N-terminal His tag and a TEV cleavage site (MGSSHHHHHHSQDPENLYFQ) before Gly728. Using this co-expression construct, the His-VgrG3C–TsiV3 complex was expressed in *E. coli* BL21-CodonPlus(DE3)-RIPL strain and purified to homogeneity. The dialyzed proteins were subjected to limited proteolysis using subtilisin from the Proti-Ace Kit (Hampton Research) at an enzyme:substrate ratio of 1:10 000 at 4°C overnight. Nonspecific proteases such as subtilisin may be more effective in obtaining crystallizable truncations under certain circumstances (Mandel *et al.*, 2006). The digested complex was further purified on a 5 ml anion-exchange HiTrap Q column (GE Healthcare). The purified complex was concentrated and loaded onto a HiLoad Superdex 200 size-exclusion column (GE Healthcare) in 150 m*M* NaCl, 20 m*M* Tris–HCl pH 7.9. The peak fractions were collected and concentrated to ∼20 mg ml^{-1} for crystallization.

Table 1
Data-collection, phasing and refinement statistics for the VgrG3C^{CD}–TsiV3 complex.

Values in parentheses are for the highest resolution shell.

Data collection	
Space group	$P2_1$
Wavelength (Å)	0.9789
Resolution (Å)	29.5–2.3 (2.34–2.30)
Unit-cell parameters (Å, °)	a = 52.0, b = 116.0, c = 68.2, α = 90, β = 94.1, γ = 90
Unique reflections	36203 (1827)
$\langle I/\sigma(I)\rangle$	28.0 (4.9)
Completeness (%)	100 (100)
R_{merge} (%)	7.2 (42.2)
Wilson B factor (Å^2)	25.15
Structure refinement	
R_{work} (%)	18.6
R_{free} (%)	23.4
Average B factors (Å^2)	
Protein	20.19
Water	26.25
Total	20.52
Root-mean-square deviations	
Bond lengths (Å)	0.010
Bond angles (°)	1.284
Ramachandran plot	
Most favoured (%)	93.3
Additionally allowed (%)	6.7

2.2. Crystallization and data collection

Native and selenomethionine-substituted (SeMet) crystals of the VgrG3C–TsiV3 protein complex were obtained and optimized in 15%(*w*/*v*) PEG 8000, 0.1 *M* sodium cacodylate pH 5.6, 0.2 *M* magnesium acetate using the hanging-drop vapour-diffusion method at 16°C. The dynamic seeding method was employed to optimize the crystal quality (Zhu *et al.*, 2005). Crystals normally appeared in 2–3 d and grew to full size in one to two weeks. For cryoprotection, crystals were soaked in reservoir solution supplemented with 25% xylitol for a few seconds and were then flash-cooled in liquid nitrogen before being taken to a synchrotron-radiation source for data collection. Diffraction data were collected on beamline 3W1A at BSRF (Beijing Synchrotron Radiation Facility) with a MAR165 CCD detector and were processed with *HKL*-2000 (Otwinowski & Minor, 1997)

2.3. Structure determination and refinement

The crystal belonged to space group $P2_1$, with two VgrG3C^{CD}–TsiV3 complexes in the asymmetric unit. The phase was determined by the single anomalous dispersion method (SAD) based on the SeMet protein crystals. Electron-density maps were calculated using *PHENIX* (Adams *et al.*, 2010; McCoy *et al.*, 2004, 2007). Model building was carried out using *Coot* (Emsley *et al.*, 2010) and refinement was performed

[1] Supporting information has been deposited in the IUCr electronic archive (Reference: RR5063).

with *REFMAC* (Murshudov *et al.*, 2011) and *PHENIX* (Adams *et al.*, 2010; McCoy *et al.*, 2004, 2007). The final R_{work} and R_{free} values were 0.186 and 0.234, respectively. The final structure was analyzed with *PROCHECK* (Laskowski *et al.*, 1993). Data-collection and refinement statistics are presented in Table 1. Structure figures were prepared using *PyMOL* (http://www.pymol.org) and the coordinates have been deposited in the PDB under accession code 4noo.

2.4. Surface plasmon resonance (SPR) analysis

The interaction kinetics between VgrG3C and wild-type and mutant TsiV3 were examined using CM5 sensor chips on a Biacore T100 (GE Healthcare) at 25°C. The running buffer [20 m*M* HEPES pH 7.5, 150 m*M* NaCl, 0.5%(*v*/*v*) Tween 20] was vacuum-filtered and degassed immediately prior to use. Ligands at ∼5 µg ml^{-1} in 10 m*M* sodium acetate pH 5.5 were immobilized to 500 response units on the flow cell. The remaining binding sites were blocked by 1 *M* ethanolamine pH 8.5. Analytes of the wild type and mutants were injected over the chip surface immobilized with ligands at a flow rate of 40 µl min^{-1}. After each cycle, the surface was regenerated by a 20 s wash with 20 m*M* NaOH. Data were analyzed by kinetic analysis with the *Biacore T100* evaluation software using a 1:1 Langmuir binding model.

2.5. Lysis assay

Mid-log cultures were harvested and resuspended to an OD_{600} of ∼1.0 in 20 m*M* HEPES pH 7.5. Aliquots of 200 µl were transferred to a 96-well plate and the absorbance at 600 nm was recorded after 20 min incubation at 37°C. A 10 µl volume of protein sample was added to each well. 1 mg ml^{-1} polymyxin B was used to permeabilize the outer membranes. The decrease in the OD_{600} subtracted from the background absorbance was compared with buffer control (assumed as 100%) to determine the percentage lysis mediated by VgrG3C.

2.6. Gel-filtration chromatography

Gel-filtration chromatography was performed following a previous protocol (Wang, Li *et al.*, 2013) using a Superdex 75 column on an ÄKTApurifier 10 (GE Healthcare). The column was equilibrated with two column volumes of buffer *A* (20 m*M* HEPES pH 7.5, 150 m*M* NaCl). Samples were fractionated at a flow rate of 0.5 ml min^{-1} and collected as 1.0 ml fractions after injection into the column. Protein fractions were separated by 15% SDS–PAGE.

2.7. *E. coli* toxicity assay

E. coli cultures were serially diluted in LB and spotted onto LB agar with 0.03 m*M* IPTG plus antibiotics (ampicillin and kanamycin). Various constructs of VgrG3C^{CD} and TsiV3 were cloned into pET-26b and pET-22b vectors, respectively, and were co-transformed into *E. coli* BL21(DE3)pLysS competent cells. Single colonies were picked for overnight culture at 37°C. The cells were then serially diluted tenfold and a 2 µl culture of each dilution was dotted onto an LB agar plate cultured at 37°C. Pictures were taken after incubation for 20–26 h.

2.8. Enzymatic analysis by HPLC

VgrG protein and its mutants were incubated with murein in buffer containing 20 m*M* Tris pH 7.5 for 12 h at room

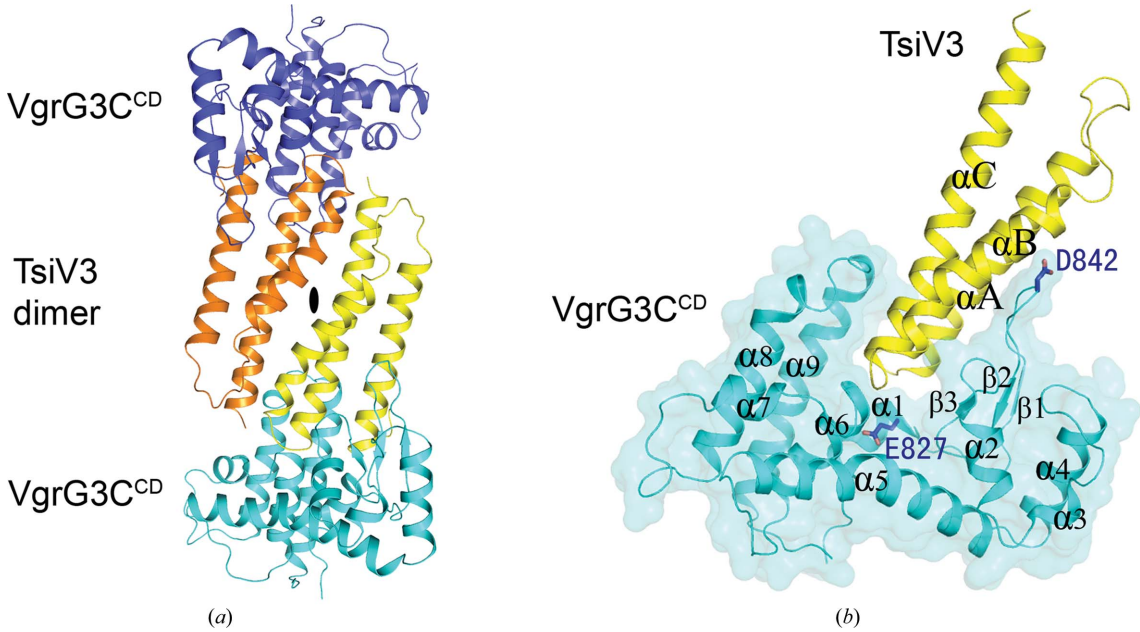

Figure 1
Structure of the VgrG3C^{CD}–TsiV3 complex. (*a*) Overall structure of the VgrG3C^{CD}–TsiV3 complex. The heterotetramer complex in the asymmetric unit is composed of one TsiV3 homodimer (subunit I, yellow; subunit II, orange) and two VgrG3C^{CD} molecules (cyan and blue). The twofold symmetry axis is marked as a black oval. (*b*) A deep groove between the two domains of VgrG3C^{CD} is formed and TsiV3 is inserted into the groove of VgrG3C^{CD}. The catalytic residues Glu827 and Asp842 are shown as sticks in deep blue.

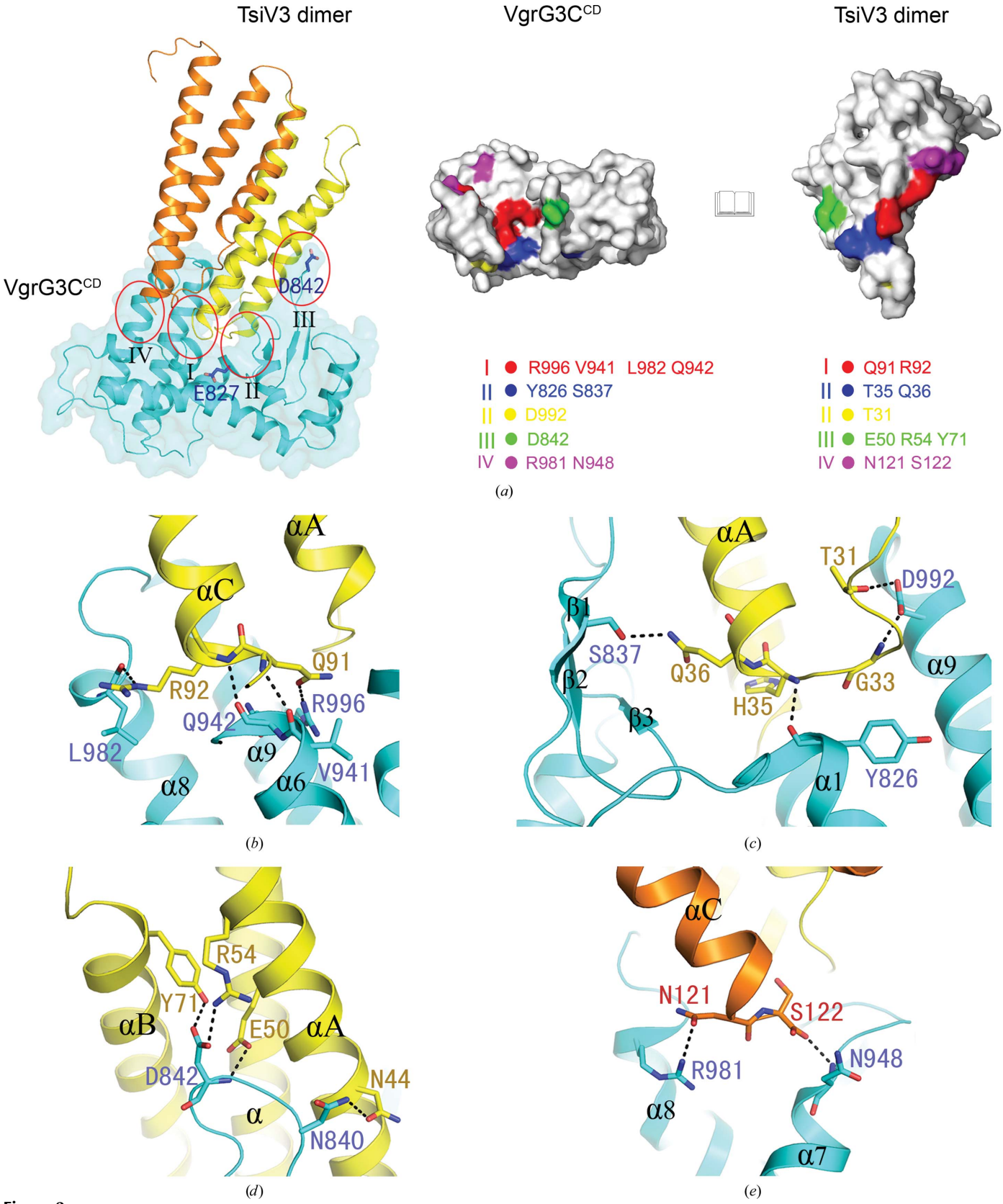

Figure 2
The interactions between VgrG3C^{CD} and TsiV3. (*a*) The interaction between the TsiV3 dimer and one VgrG3C^{CD} molecule. Four interacting regions (I–IV) are highlighted by red circles. (*b*) Open-book view. VgrG3C^{CD} and TsiV3 were rotated in reverse directions horizontally 75° around the *y* axis and were then rotated −60° around the *x* axis. The interacting residues in region I are indicated in red, those in region II in blue and yellow, those in region III in green and those in region IV in purple. (*c*–*e*) Close-up views showing interactions in regions I (*c*), II (*d*), III (*e*) and IV (*f*) at the VgrG3C^{CD}–TsiV3 interface.

temperature. The reaction was then stopped by heat treatment followed by centrifugation. The obtained supernatant (muropeptides) was reduced with sodium borohydride. Before application to HPLC, the reduced muropeptides were filtered through a 0.22 µm membrane. Finally, the degraded muropeptides were separated on a VP-ODS column (150 × 4.6 mm, Shimadzu) using a linear gradient from 50 m*M* sodium phosphate pH 4.3 to 75 m*M* sodium phosphate pH 4.8 and 15% methanol at a flow rate of 0.5 ml min^{-1} for 135 min. The effluent was monitored by UV at 205 nm.

2.9. Analytical untracentrifugation

Sedimentation-velocity measurements were performed on a ProteomeLab XL-I (Beckman) at 25°C. All protein samples were diluted to an $OD_{280\ nm}$ of 0.8 in 20 m*M* HEPES pH 7.5, 150 m*M* NaCl. Data were collected at 60 000 rev min^{-1} (262 000*g*) every 3 min at a wavelength of 280 nm. Interference sedimentation-coefficient distributions, $c(M)$, were calculated from the sedimentation-velocity data using *SEDFIT* (Schuck, 2000).

2.10. Statistical analysis

Student's *t*-test was used in statistical analysis using *SigmaPlot*.

3. Results

3.1. Structure of the VgrG3C^{CD}–TsiV3 complex

We co-expressed VgrG3C (residues 728–1017) with TsiV3 (residues 25–122) and purified the recombinant complex to homogeneity. However, successful crystallization required a limited proteolysis procedure of the complex which deleted the PGB domain (VgrG3C^{PGB}; residues 728–812), leaving the C-terminal catalytic domain (VgrG3C^{CD}; residues 813–1017) intact and in complex with TsiV3. The crystal structure of the VgrG3C^{CD}–TsiV3 complex was determined by the single-wavelength anomalous diffraction (SAD) method at 2.3 Å resolution. There are two copies of the complex in the asymmetric unit (Fig. 1*a*). The final atomic model includes residues 816–1015 of VgrG3C^{CD} and residues 28–122 of TsiV3. The model has good agreement with the crystallographic data and the expected geometric parameters (Table 1).

The VgrG3C^{CD}–TsiV3 complex is an $\alpha_2\beta_2$ heterotetramer, consistent with the results from gel-filtration experiments (data not shown). A TsiV3 dimer is located in the centre of the complex, and the two VgrG3C^{CD} domains are bound at the distal ends of the TsiV3 dimer (Fig. 1*a*).

The structure of VgrG3C^{CD} contains nine α-helices (α1–α9) and a three-stranded β-sheet (β1–β3) (Fig. 1*b*). The structure forms two domains connected by a bent α5 helix. There is a deep groove between the two domains, which is the binding site for TsiV3 as well as the active site of VgrG3C^{CD}.

The structure of the TsiV3 monomer contains a three-helical bundle (αA–αC; Fig. 1*b*). There are two disulfide bonds in the structure, Cys28–Cys41 and Cys82–Cys100, and these Cys residues are conserved among TsiV3 homologues. The two TsiV3 monomers are arranged in a head-to-tail fashion in the dimer, with helices αB and αC in the interface (Figs. 1*a* and 1*b*).

3.2. The interactions between VgrG3C^{CD} and TsiV3

The interactions between VgrG3C^{CD} and TsiV3 are primarily mediated by the three-helical bundle of TsiV3 inserting into the deep groove in the structure of VgrG3C^{CD} (Fig. 2*a*). The second monomer of the TsiV3 dimer also contributes to the dimer interface. The total buried surface area between the TsiV3 dimer and one VgrG3C^{CD} molecule is 1490 Å^2, with 1270 Å^2 contributed by one monomer of TsiV3 and 220 Å^2 by the other monomer.

The VgrG3C^{CD}–TsiV3 interface can be divided into four regions: I–IV (Fig. 2*a*). The first three regions involve one monomer of TsiV3, while region IV involves the other monomer. In region I, Gln91 and Arg92 at the N-terminus of the αC helix of TsiV3 form four main-chain and side-chain hydrogen bonds to VgrG3C^{CD} [Figs. 2*b* (red) and 2*c*]. In region II, several residues on the N-terminal loop and the N-terminus of the αA helix of TsiV3 interact with VgrG3C^{CD} via a number of hydrogen bonds [Figs. 2*b* (blue and yellow) and 2*d*]. Region III involves interactions between the αA helix of TsiV3 and the β1–β2 loop of VgrG3C [Figs. 2*b* (green) and 2*e*]. Finally, interactions in region IV are mediated by the C-terminal end of TsiV3, residues Asn121 and Ser122. In particular the C-terminal carboxylate group of Ser122 makes one hydrogen bond to VgrG3C^{CD} [Figs. 2*b* (purple) and 2*f*].

3.3. VgrG3C^{CD} adopts a chitosanase fold

VgrG3C^{CD} shares structural similarity with chitosanases from *Streptomyces* N174 (PDB entry 1chk; *Z*-score 11.6; Marcotte *et al.*, 1996) and *Bacillus circulans* MH-K1 (PDB entry 1qgi; *Z*-score 11.0; Saito *et al.*, 1999) (Figs. 3*a* and 3*b*), although the sequence identities between them are only 15.5 and 10.0%, respectively. The r.m.s. deviations are 3.1 Å for 168 aligned C$^\alpha$ atoms between VgrG3C^{CD} and the chitosanase from *Streptomyces* N174 and 2.9 Å for 159 aligned C$^\alpha$ atoms between VgrG3C^{CD} and the chitosanase from *B. circulans* MH-K1. There are also large structural differences between VgrG3C^{CD} and these other enzymes, which are especially apparent for helix α3 in VgrG3C (Fig. 1*b* and Fig. 3*a*). Structural variation in this region may be a distinguishing feature of these chitosanases.

The active sites of chitosanases contain a catalytic dyad of Glu and Asp residues, which are conserved in VgrG3C^{CD} as Glu827 and Asp842 (Dong *et al.*, 2013). Glu827 is located in helix α1 at the bottom of the large groove between the two domains of VgrG3C^{CD} (Fig. 3*b*). Asp842 is in the β1–β2 loop and also in the interface with TsiV3 (region III; Fig. 2*e*). To confirm the importance of these two residues for the catalytic activity of VgrG3C, we tested the activities of E827Q and D842N mutants in the hydrolysis of peptidoglycan. The E827Q mutation completely abolished the enzymatic activity, while the D842N mutant retained residual activity (Fig. 3*c*), indicating that Glu827 has a more important role than Asp842

in the enzymatic catalysis of VgrG3C. Additionally, we found that VgrG3C^{CD} had enzymatic activity that was comparable to that of VgrG3C (data not shown).

3.4. Gln91 and Arg92 of TsiV3 are important for the recognition of VgrG3C

To assess the structural observations on the VgrG3C–TsiV3 complex, we introduced mutations in the interface and tested their effects on the stability of the complex by surface plasmon resonance (SPR) experiments. The binding affinity (K_d) between wild-type VgrG3C (WT-VgrG3C) and wild-type TsiV3 (WT-TsiV3) is 4.9 n*M* (Table 2 and Fig. 4*a*), indicating strong binding between the two proteins, and is consistent with the structure. The Q91A/R92A double mutant of TsiV3 (in region I of the interface; Fig. 2*c*) also greatly reduced the binding affinity (62-fold increase in K_d; Table 2 and Fig. 4*a*), indicating that these two residues play an important role in VgrG3C–TsiV3 recognition.

Table 2
Surface plasmon resonance (SPR) analysis of the interactions between VgrG3C and TsiV3.

		Association rate	Dissociation rate	Binding affinity
Analyte	Ligand	k_{on} (M^{-1} s^{-1})	k_{off} (s^{-1})	K_d (n*M*)
WT-TsiV3	VgrG3C	2.04×10^5	1.00×10^{-3}	4.92
T31A-TsiV3	VgrG3C	3.72×10^5	5.39×10^{-3}	14.50
H35A/Q36A-TsiV3	VgrG3C	5.34×10^5	12.19×10^{-3}	22.82
N44A-TsiV3	VgrG3C	2.12×10^5	0.95×10^{-3}	4.49
Q91A/R92A-TsiV3	VgrG3C	0.29×10^5	8.94×10^{-3}	307.09
Δ120-TsiV3	VgrG3C	2.18×10^5	0.50×10^{-3}	2.31
Y85A/Y111A-TsiV3	VgrG3C	14.63×10^5	47.39×10^{-3}	32.40
WT-VgrG3C	TsiV3	4.65×10^5	1.33×10^{-3}	2.86
D842L-VgrG3C	TsiV3	3.16×10^5	3.89×10^{-3}	12.31

The T31A and H35A/Q36A mutations of TsiV3 (region II; Fig. 2*d*) led to 2.9-fold and 4.6-fold reductions in the binding affinity, respectively, while the N44A mutation (region III; Fig. 2*e*) had no effect on the interaction (Table 2 and Supplementary Fig. S2). To assess the importance of region IV

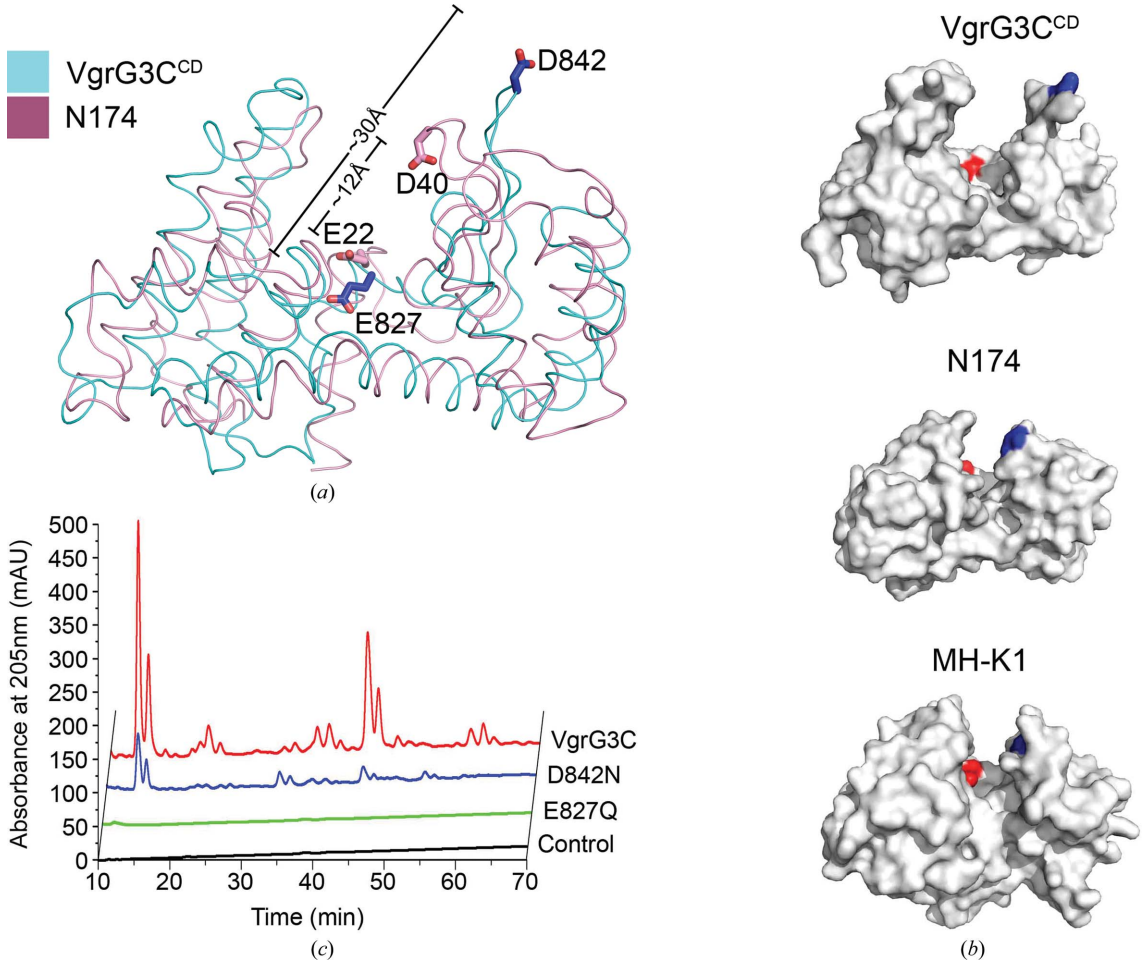

Figure 3
VgrG3C^{CD} adopts a chitosanase fold. (*a*) Structural superpositions of VgrG3C^{CD} (cyan) with *Streptomyces* N174 (dark salmon) chitosanase. The catalytic residues are labelled and shown in stick representation. (*b*) Surface view illustrating the differences in the pocket size between VgrG3C^{CD} deducted from the complex and *Streptomyces* N174 and *B. circulans* MH-K1 chitosanase in the apo form. The catalytic glutamic acid is coloured red, while the catalytic aspartic acid is coloured blue. (*c*) Mutation of dyad residues impairs the enzymatic activity of VgrG3C. HPLC chromotograms of soluble peptidoglycan products detected after 12 h incubation with enzymatic proteins. VgrG3C^{CD} had an enzymatic activity that was comparable to that of VgrG3C (data not shown). The data represent three independent experiments.

(Fig. 2*f*), we deleted the last two residues (Asn121 and Ser122) of TsiV3 (Δ120 mutant). The mutant displayed almost equal affinity for WT-VgrG3C (Table 2 and Supplementary Fig. S2), suggesting that this interface is dispensable for binding. We also mutated the Asp842 residue of the catalytic dyad of VgrG3C, which interacts with Glu50, Arg54 and Tyr71 of TsiV3 (region III; Fig. 2*d*). The D842L mutation caused a 4.3-fold reduction in the binding affinity (Table 2 and Supplementary Fig. S2), indicating that the interactions in interface region III play an accessory role in VgrG3C–TsiV3 recognition.

We next examined the inhibitory activities of the TsiV3 mutants on the toxicity of VgrG3C in cells. We expressed VgrG3C^{CD} with TsiV3 wild type and mutants all tagged with an N-terminal periplasmic secretion signal peptide in *E. coli*. We observed that VgrG3C^{CD} with the secretion signal was toxic (Fig. 4*b*). However, WT-TsiV3 was able to block this toxicity, allowing the cells to grow. In accordance with the SPR data, the T31A, H35A/Q36A and Q91A/R92A mutants all significantly impaired the inhibitory activities of TsiV3 on VgrG3C^{CD} in cells, while the N44A mutant had normal inhibitory activity (Fig. 4*b*). Overall, our data confirmed the structural observations on the complex and showed that Arg91 and Gln92 of TsiV3 are important for the recognition of its effector VgrG3 in *V. cholerae*.

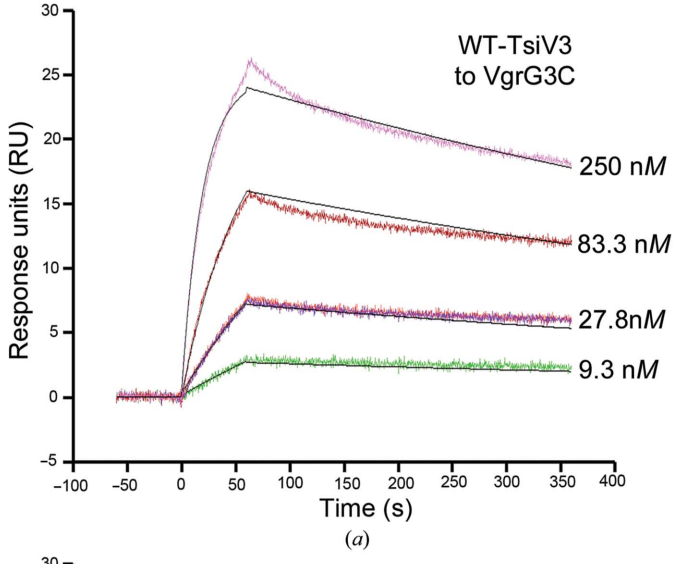

(*a*)

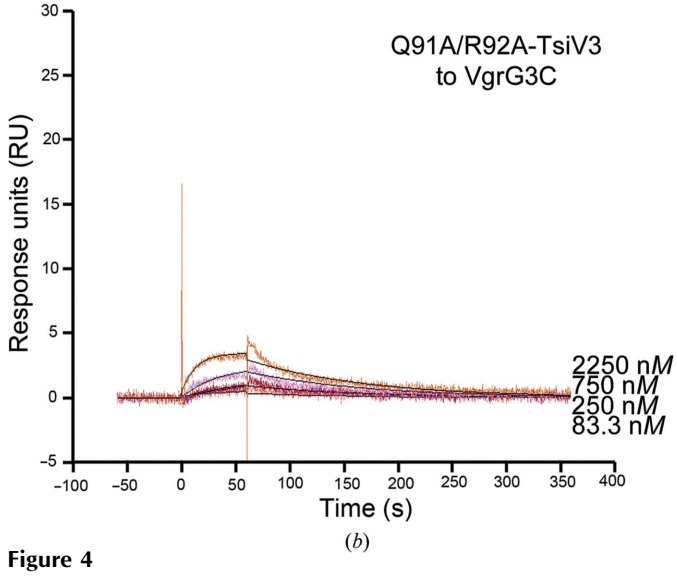

(*b*)

3.5. Dimerization of TsiV3 is critical for its inhibitory activity

Helices αB and αC contribute to the dimerization of TsiV3. Side chain-mediated hydrogen bonds are formed between Arg92 and Ser122, between Asn87 and Tyr115, between Tyr85 and Asp118 (sites I and I′; Figs. 5*a* and 5*b*) and between Glu80 and Arg73 (sites II and II′; Figs. 5*a* and 5*b*). Additional hydrogen bonds are also formed between the side chains of Arg92, Tyr111 and Gln74 and the main chains of Asn87, Lys81 and Ala77, respectively. As the two monomers are arranged in a head-to-tail fashion in the dimer, the hydrogen bonds of the dimer are duplicated, giving a total of 14 hydrophilic interacting pairs (Figs. 5*a* and 5*b*).

The dimer interface of TsiV3 buries 1070 Å^2 of the surface area of the monomers. TsiV3 behaves as a dimer on size-exclusion chromatography (data not shown). An analytical ultracentrifugation experiment shows a calculated molecular mass of 23.4 kDa, close to the theoretical dimeric molecular weight of a TsiV3 dimer (24.3 kDa) (Supplementary Fig. S3), indicating that TsiV3 exists as a dimer in solution.

To examine the importance of TsiV3 dimerization for its inhibitory activity, we first tried to separate the dimer into monomers. Based on our structural analysis, four residues, Lys73, Tyr85, Tyr111 and Tyr115, contributing significantly to dimerization, were selected for alanine substitution. However, these four mutations had no effect on TsiV3 dimerization, probably owing to the robustness of the hydrogen-bonding network in the dimer interface. Hence, two double mutants, K73A/Y111A and Y85A/Y111A, were generated and we found that the Y85A/Y111A mutant abolished TsiV3 dimerization on size-exclusion chromatography (data not shown).

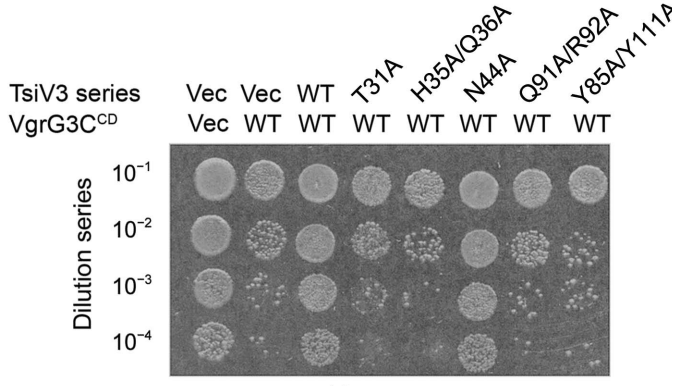

(*c*)

Figure 4
Gln91 and Arg92 of TsiV3 are important for the recognition of VgrG3C. (*a*) Surface plasmon resonance (SPR) data of VgrG3C binding to wild-type (WT) and R91A/Q92A mutant TsiV3. (*b*) Toxic lysis of *E. coli* by different mutants. *E. coli* strains were co-expressed with TsiV3 series in pET-22b vector and VgrG3C^{CD} was expressed in pET-26b vector, with N-terminal periplasmic localization signal peptides for all proteins. Vec, vector control; WT, wild type. Data are representative of at least three separate experiments.

Consistent with the size-exclusion results, wild-type TsiV3 and the Y85A/Y111A mutant showed calculated molecular masses of 23.4 and 13.8 kDa, respectively, in analytical ultracentrifugation experiments (Supplementary Fig. S3).

We then characterized the interaction between the monomeric Y85A/Y111A TsiV3 mutant and VgrG3C by SPR experiments. We found that the mutant had a reduced affinity for VgrG3C, with a K_d of 32.4 n*M* (Table 2). Consistent with the SPR data, our functional experiments showed that the mutant also failed to inhibit the toxicity of VgrG3C in *E. coli* cells (Figs. 4*b* and 5*e*). Taken together, the data suggest that the dimerization of TsiV3 is important for the stability of the VgrG3C–TsiV3 complex and is critical for the disruption of the enzymatic activity of VgrG3C.

4. Discussion

Our structure of the VgrG3C–TsiV3 complex reveals the molecular basis for the inhibition of VgrG3C catalytic activity by TsiV3. First of all, the TsiV3 dimer is bound in the active-site region of VgrG3C^{CD}, thereby blocking it from interacting with any substrates. Moreover, the binding of TsiV3 causes a significant distortion of the catalytic dyad, such that its residues are not capable of catalysis even if substrates were able to bind. In the structures of the chitosanases from *Streptomyces* N174 and *B. circulans* MH-K1, the two residues of the dyad face each other and are located within 12 Å (Fig. 3*a*). In comparison, the $\beta1$–$\beta2$ loop (containing Asp842) is pushed away from the active-site groove and the Glu827 residue is pushed deeper into the base of the groove, such that they are separated by ∼30 Å in the TsiV3 complex (Fig. 3*a*).

The T6SS apparatus is a long tubular structure composed of an inner tube formed of multiple copies of the Hcp protein and an external contractile sheath consisting of VipA and VipB proteins (Basler & Mekalanos, 2012; Silverman *et al.*, 2012; Supplementary Fig. S1). The bacterial T6SS organelle is functionally similar to the contractile tails of bacteriophages (Leiman *et al.*, 2009; Silverman *et al.*, 2012). Rapid contraction of the sheath causes release of the inner tube toxic effectors of the predatory cell into a prey cell. VgrG proteins form a trimeric spike positioned at the end of the tube (Supplementary Fig. S1). Moreover, VgrG proteins contain C-terminal extension effectors that are toxic (Pukatzki *et al.*, 2007; Brooks *et al.*, 2013) and may also associate with other effector molecules (Dong *et al.*, 2013). Shneider and coworkers replaced the tip of the gp5 β-helix with the equivalent last two β-helices of VgrG proteins to generate gp5-VgrG chimeras and co-expressed them with PAAR proteins for crystallization (Shneider *et al.*, 2013). The gp5(VCA0018)–VCA0105 complex forms a symmetrical cone-shaped structure. The PAAR proteins associate with the VgrG β-helix through a flat hydrophobic patch consisting of 14 or 16 hydrogen bonds, which forms a perfect triangle connecting the central hydrophobic patch acting as a spike needle. Here, we show that the C-terminal extension of VgrG3 with a deletion of its PGB domain (VgrG3C^{CD}) can bind to its immunity partner TsiV3 to inactivate its effector function. VgrG3C^{CD} still has enzymatic activity. However, whether VgrG3 dynamically binds to PAAR proteins for killing or to immunity pairs for self-protection needs to be further investigated.

Two representative members Tge1^{PA} (Wang, Ding *et al.*, 2013; Li *et al.*, 2013) and Tge2^{PP} (Whitney *et al.*, 2013) of the T6SS muramidase Tge (type VI secretion glycoside hydrolase effectors) superfamily have recently been crystallized in complex with their cognate immunity proteins Tgi1^{PA} and Tgi2^{PP}, respectively. The C-terminal catalytic domain of Tge1^{PA} adopts a soluble lytic transglycosylase (SLT) fold (Li *et al.*, 2013; Wang, Ding *et al.*, 2013), while Tge2^{PP} closely resembles members of glycoside hydrolase family 73 (GH73; Whitney *et al.*, 2013). Based on our structure, we found that VgrG3C harbours the chitosanase fold, which is reminiscent of the chitosanases from *Streptomyces* N174 (Marcotte *et al.*, 1996) and *B. circulans* MH-K1 (Saito *et al.*, 1999). VgrG3C

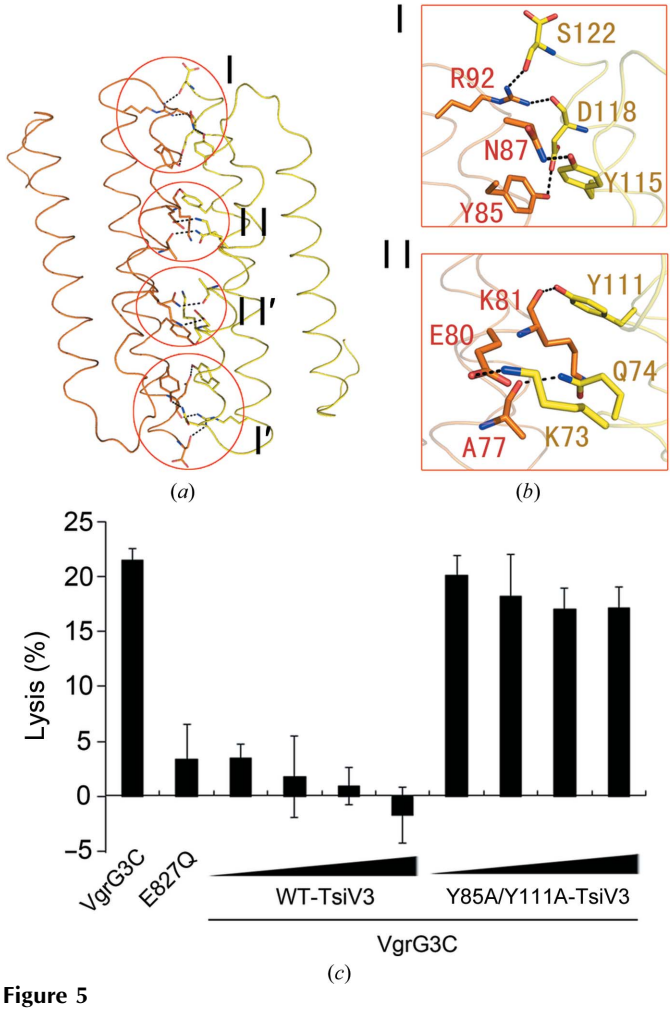

Figure 5
Dimerization of TsiV3 is critical for its inhibitory activity. (*a*, *b*) Side view of the TsiV3 dimer. Interacting residues at the interface of the TsiV3 dimer are labelled and shown in stick representation. Details of interfaces I and II are enlarged. Interfaces I′ and II′ are symmetric to interfaces I and II. (*c*) The Y85A/Y111A-TsiV3 mutant abolishes the inhibitory function against the effector VgrG3C. Lysis was calculated based on the decrease in absorbance at $OD_{600\,nm}$ using mid-logarithmic phase *E. coli*. Different doses of WT-TsiV3 and Y85A/Y111A-TsiV3 mutant proteins were used to examine their inhibitory activities. Data are representative of at least three independent experiments.

might also catalyze the hydrolytic degradation of chitosan. However, its chitosanase activity remains to be further investigated.

We found that the dimerization of TsiV3 is essential for its inhibitory function, consistent with our crystal architecture in which two copies of the VgrG3C^{CD}–TsiV3 complex are present in the symmetric unit. Mutation of single residues that contribute to interface hydrogen-bond formation does not affect the formation of the TsiV3 dimer. However, a double mutation of both Tyr85 and Tyr111 (Y85A/Y111A mutant) disrupts the formation of the TsiV3 dimer. Additionally, the Y85A/Y111A mutant abolishes its inhibitory function against its toxic effector VgrG3C. Therefore, we conclude that the dimerization of TsiV3 is critical for its inhibitory activity against its effector partner VgrG3.

The C-terminal extension of VgrG3 contains a peptidoglycan-binding (PGB) domain (Pukatzki *et al.*, 2007, 2009), implying that VgrG3 might target the cell wall of prey prokaryotic cells for hydrolysis. Moreover, VgrG3 has been proposed to first enter the cytosol of the prey cell along with the VgrG spike in a one-step manner without a pause in the prey periplasm (Whitney *et al.*, 2013). In this scenario, redistribution to the periplasm is required for VgrG3 to exert its lytic function. However, VgrG3 causes cell rounding even when expressed in cytosol without a guiding signal peptide (Dong *et al.*, 2013). We found that the cytosolic expression of VgrG3C (residual 728–1017) did have a deleterious effect on host *E. coli* cells. In contrast, the deletion of the PGB domain completely abolished this effect in cytosol (data not shown), indicating that the PGB domain facilitates toxicity of VgrG3 *in vivo*. We found that VgrG3C^{CD} still exhibits enzymatic activity that is comparable to VgrG3C in the hydrolysis of peptidoglycan. Moreover, the periplasm-targeted VgrG3C^{CD} has a strong cytoxic effect *in vivo*, which is analogous to VgrG3C. Our structural and biochemical data define the molecular mechanism underlying the self-protection of *V. cholerae* and expand our understanding of the role of T6SS in bacterial competition.

We thank Yuanyuan Chen for assistance in SPR analysis and the staff of beamline 3W1A at Beijing Synchrotron Radiation Facility (Beijing, People's Republic of China) for technical assistance during data collection. We thank Professor David Waugh (National Cancer Institute, Frederick, Maryland, USA), Professor Steven Pascal (Massey University, Palmerston North, New Zealand) and Professor Lloyd Ruddock (University of Oulu, Finland) for providing reagents. This work was supported by the National Natural Science Foundation of China (81330047, 31128003 and 31025009), the 973 Program (2010CB911902) and the Innovative programs of Chinese Academy of Sciences (XDA01010407). XY and MX designed the study, performed experiments, analyzed data and wrote the manuscript. XY performed protein purification and crystallization, MX solved the structure and refined the model and XY, YW, PX, SW and BY contributed to the biochemical experiments and analyzed the data. ZF guided the research, LT and TJ supervised all crystallographic studies and structural analyses. ZF, LT and TJ analyzed the data and wrote the manuscript.

References

Adams, P. D. *et al.* (2010). *Acta Cryst.* D**66**, 213–221.
Basler, M. & Mekalanos, J. J. (2012). *Science*, **337**, 815.
Bingle, L. E., Bailey, C. M. & Pallen, M. J. (2008). *Curr. Opin. Microbiol.* **11**, 3–8.
Brooks, T. M., Unterweger, D., Bachmann, V., Kostiuk, B. & Pukatzki, S. (2013). *J. Biol. Chem.* **288**, 7618–7625.
Dong, T. G., Ho, B. T., Yoder-Himes, D. R. & Mekalanos, J. J. (2013). *Proc. Natl Acad. Sci. USA*, **110**, 2623–2628.
Durand, E., Derrez, E., Audoly, G., Spinelli, S., Ortiz-Lombardia, M., Raoult, D., Cascales, E. & Cambillau, C. (2012). *J. Biol. Chem.* **287**, 38190–38199.
Emsley, P., Lohkamp, B., Scott, W. G. & Cowtan, K. (2010). *Acta Cryst.* D**66**, 486–501.
English, G., Trunk, K., Rao, V. A., Srikannathasan, V., Hunter, W. N. & Coulthurst, S. J. (2012). *Mol. Microbiol.* **86**, 921–936.
Hibbing, M. E., Fuqua, C., Parsek, M. R. & Peterson, S. B. (2010). *Nature Rev. Microbiol.* **8**, 15–25.
Hood, R. D. *et al.* (2010). *Cell Host Microbe*, **7**, 25–37.
Laskowski, R. A., MacArthur, M. W., Moss, D. S. & Thornton, J. M. (1993). *J. Appl. Cryst.* **26**, 283–291.
Leiman, P. G., Basler, M., Ramagopal, U. A., Bonanno, J. B., Sauder, J. M., Pukatzki, S., Burley, S. K., Almo, S. C. & Mekalanos, J. J. (2009). *Proc. Natl Acad. Sci. USA*, **106**, 4154–4159.
Li, L., Zhang, W., Liu, Q., Gao, Y., Gao, Y., Wang, Y., Wang, D. Z., Li, Z. & Wang, T. (2013). *J. Biol. Chem.* **288**, 30607–30613.
Ma, A. T., McAuley, S., Pukatzki, S. & Mekalanos, J. J. (2009). *Cell Host Microbe*, **5**, 234–243.
MacIntyre, D. L., Miyata, S. T., Kitaoka, M. & Pukatzki, S. (2010). *Proc. Natl Acad. Sci. USA*, **107**, 19520–19524.
Mandel, C. R., Gebauer, D., Zhang, H. & Tong, L. (2006). *Acta Cryst.* F**62**, 1041–1045.
Marcotte, E. M., Monzingo, A. F., Ernst, S. R., Brzezinski, R. & Robertus, J. D. (1996). *Nature Struct. Biol.* **3**, 155–162.
McCoy, A. J., Grosse-Kunstleve, R. W., Adams, P. D., Winn, M. D., Storoni, L. C. & Read, R. J. (2007). *J. Appl. Cryst.* **40**, 658–674.
McCoy, A. J., Storoni, L. C. & Read, R. J. (2004). *Acta Cryst.* D**60**, 1220–1228.
Murshudov, G. N., Skubák, P., Lebedev, A. A., Pannu, N. S., Steiner, R. A., Nicholls, R. A., Winn, M. D., Long, F. & Vagin, A. A. (2011). *Acta Cryst.* D**67**, 355–367.
Otwinowski, Z. & Minor, W. (1997). *Methods Enzymol.* **276**, 307–326.
Patrick, A. (2013). *Lancet*, **381**, 1264.
Pukatzki, S., Ma, A. T., Revel, A. T., Sturtevant, D. & Mekalanos, J. J. (2007). *Proc. Natl Acad. Sci. USA*, **104**, 15508–15513.
Pukatzki, S., Ma, A. T., Sturtevant, D., Krastins, B., Sarracino, D., Nelson, W. C., Heidelberg, J. F. & Mekalanos, J. J. (2006). *Proc. Natl Acad. Sci. USA*, **103**, 1528–1533.
Pukatzki, S., McAuley, S. B. & Miyata, S. T. (2009). *Curr. Opin. Microbiol.* **12**, 11–17.
Russell, A. B., Singh, P., Brittnacher, M., Bui, N. K., Hood, R. D., Carl, M. A., Agnello, D. M., Schwarz, S., Goodlett, D. R., Vollmer, W. & Mougous, J. D. (2012). *Cell Host Microbe*, **11**, 538–549.
Saito, J., Kita, A., Higuchi, Y., Nagata, Y., Ando, A. & Miki, K. (1999). *J. Biol. Chem.* **274**, 30818–30825.
Schuck, P. (2000). *Biophys. J.* **78**, 1606–1619.
Shneider, M. M., Buth, S. A., Ho, B. T., Basler, M., Mekalanos, J. J. & Leiman, P. G. (2013). *Nature (London)*, **500**, 350–353.
Silverman, J. M., Brunet, Y. R., Cascales, E. & Mougous, J. D. (2012). *Annu. Rev. Microbiol.* **66**, 453–472.
Vezzulli, L., Guzmán, C. A., Colwell, R. R. & Pruzzo, C. (2008). *Curr. Opin. Biotechnol.* **19**, 254–259.
Wang, T., Ding, J., Zhang, Y., Wang, D.-C. & Liu, W. (2013). *Acta Cryst.* D**69**, 1889–1900.

Wang, L., Li, Q., Wu, L., Liu, S., Zhang, Y., Yang, X., Zhu, P., Zhang, H., Zhang, K., Lou, J., Liu, P., Tong, L., Sun, F. & Fan, Z. (2013). *J. Immunol.* **190**, 1319–1330.
Whitney, J. C., Chou, S., Russell, A. B., Biboy, J., Gardiner, T. E., Ferrin, M. A., Brittnacher, M., Vollmer, W. & Mougous, J. D. (2013). *J. Biol. Chem.* **288**, 26616–26624.
Zhu, D.-Y., Zhu, Y.-Q., Xiang, Y. & Wang, D.-C. (2005). *Acta Cryst.* D**61**, 772–775.